Ab initio quasiharmonic equations of state for dynamically stabilized soft-mode materials

N. D. Drummond and G. J. Ackland
Department of Physics and Astronomy, The University of Edinburgh, JCMB, The King's Buildings, Edinburgh, United Kingdom
(Received 29 October 2001; revised manuscript received 30 January 2002; published 25 April 2002)

We introduce a method for treating soft modes within the analytical framework of the quasiharmonic equation of state. The corresponding double-well energy-displacement relation is fitted to a functional form that is harmonic in both the low- and high-energy limits. Using density-functional calculations and statistical physics, we apply the quasiharmonic methodology to solid periclase (MgO). We predict the existence of a $B1$-$B2$ phase transition at high pressures and temperatures.

DOI: 10.1103/PhysRevB.65.184104 PACS number(s): 61.50.Ks, 64.70.Kb, 71.20.−b

I. INTRODUCTION

The quasiharmonic approximation[1] provides a means of extracting finite-temperature properties of materials from static calculations. It assumes that the vibrational properties can be understood in terms of excitations of noninteracting harmonic normal modes: *phonons*. Lattice dynamics[2] can be used to calculate phonon energies by evaluating the eigenvalues of the dynamical matrix, which involves second derivatives of the crystal energy with respect to atomic displacements.

The frequencies of these modes depend on the crystal's density. Hence they have a temperature dependence that arises simply because of thermal expansion in the material.

Recent developments in *ab initio* energy calculations have enabled full phonon dispersion curves to be obtained, leading to a resurgence of interest in the quasiharmonic approach. Difficulties arise, however, when the dynamical matrix has negative eigenvalues, indicating that the crystallographic structure is not a local minimum of energy. Such crystals may be *dynamically stabilized*: because of their large entropy, they may represent a minimum of free energy at high temperature. Within the conventional assumption of harmonic phonons, the quasiharmonic framework leads to divergent free energies in these cases. Such systems have been treated numerically from first principles using Monte Carlo methods with effective Hamiltonians[3] or molecular-dynamics simulations of a reduced set of modes.[4] Here we relax the quasiharmonic assumption of harmonic modes while retaining the approximation of noninteracting phonons, and show how the intrinsic anharmonicity of such modes can be included in analytic free-energy calculations.

The mineral *periclase* (MgO) is of some geological significance as one of the supposed constituents of the Earth's lower mantle. It is generally believed that along the geotherm—the conditions of pressure and temperature actually occurring in the mantle—periclase remains in a single phase. Under other conditions, however, previous calculations have suggested that periclase has two phases in its solid state: a sodium chloride-like face-centered-cubic phase ($B1$) and a cesium chloride-like simple cubic phase ($B2$) that is favored at extremely high pressures.[5]

Imaginary phonon frequencies are found in the $B2$ phase of periclase, and have attracted enormous attention in the other principal constituent of the lower mantle, magnesium silicate perovskite ($MgSiO_3$).[6–10] Equilibrium structures, thermodynamic properties, and compositions depend on the free energy. Here we present a calculation of the free energy of periclase as a function of density and temperature. We use the pseudopotential-plane-wave approach to evaluate total energies and the method of finite displacements to evaluate pressure-dependent force constants,[11] including effective charges and dielectric constants[12] for the longitudinal optic modes. Based on calculated phonon frequencies and the quasiharmonic approximation, we present a first-principles calculation of the phase diagram and thermodynamic equation of state of solid periclase: the relationship between pressure, density, and temperature.

II. QUASIHARMONIC METHOD

A. *Ab initio* calculation of specific Helmholtz free energies

The first stage of the calculation is to obtain the specific (with respect to mass) Helmholtz free energy of each phase as a function of density and temperature. We write the free energy as the sum of the frozen-ion interaction energy and the free energy due to lattice vibrations.

1. Frozen-ion energy

The frozen-ion energy—the interaction energy of the crystal with the ions fixed in their equilibrium positions—is, by definition, temperature independent. Hence the free energy is simply equal to the internal energy. In order to determine the dependence on density, total-energy density-functional calculations are carried out for each phase at a range of different lattice parameters.

2. Lattice thermal Helmholtz free energy

We calculate the lattice thermal Helmholtz free energy of each phase as a function of density and temperature within the framework of the harmonic approximation.[13]

For a range of lattice parameters, we evaluate the matrix of force constants for a supercell (several unit cells) of the phase under consideration, subject to periodic boundary conditions. We evaluate the forces on the ions in a crystal when one ion is displaced slightly from its equilibrium position: from such calculations the matrix of force constants may be constructed.[11]

We denote the matrix of force constants by ϕ, where $\phi_{l,n,\alpha;m,p,\beta}$ is the component of force in direction α on ion n in unit cell l when ion p in unit cell m is displaced infinitesimally in direction β, divided by the magnitude of the displacement.

Pairs of density-functional calculations are carried out with an ion displaced from equilibrium along one of the Cartesian axes by a small amount in first a positive sense and then a negative sense. By averaging the resulting Hellmann-Feynman forces on the ions from the first simulation with the negative of the forces from the second, first-order anharmonic contributions to the force constants are eliminated.

The set of rotations under which the crystal structure is invariant are identified and the rotation matrices, together with the mappings between the ions under the symmetry operations, are evaluated. For a given pair of ions (l,n) and (m,p), the matrix of force constants $\phi_{l,n,\alpha;m,p,\beta}$ transforms as a second-rank tensor. However, for a symmetry operation, the transformed matrix must be the same as the (unrotated) matrix of force constants between the pair of ions which are mapped to (l,n) and (m,p). Hence new elements of the matrix of force constants can be obtained by an application of these point symmetries. Translational symmetries can be identified and exploited in a similar fashion.

The matrix of force constants should be symmetric,[13] and Newton's third law must be satisfied: if an ion is displaced slightly then the restoring force on that ion must be equal and opposite to the total force on all of the other ions. Hence we must have

$$\phi_{l,n,\alpha;m,p,\beta} = \phi_{m,p,\beta;l,n,\alpha}, \tag{1}$$

$$\phi_{l,n,\alpha;l,n,\beta} = -\sum_{(m,p)\neq(l,n)} \phi_{l,n,\alpha;m,p,\beta}. \tag{2}$$

The force constants are obtained from separate numerical calculations; hence small violations of these requirements may occur. These two conditions are therefore alternately imposed on the matrix of force constants until further application leaves the matrix unchanged.[11]

The next stage of the calculation involves the construction of dynamical matrices[13] for various wave vectors in the first Brillouin zone. A diagonalization of the dynamical matrix for a given wave vector gives the spectrum of corresponding eigenfrequencies. Strictly, these are only exact when the wavelengths are commensurate with the dimensions of the supercell.[11] However, provided that the resulting dispersion curves are smooth, it may be assumed that the interpolation errors are negligible.

Cochran and Cowley[14] have shown that the elements of the dynamical matrix for an ionic crystal can be written as the sum of a term that behaves analytically as the wave vector tends to zero, and a term that is nonanalytic at the zone center. The latter term vanishes as the boundary of the Brillouin zone is approached. This term arises because longitudinal-optic (LO) phonons cause an electric polarization field to be set up within the crystal as the oppositely charged ions are displaced in opposite directions. The resulting long-range interactions cannot be calculated within the framework we have described so far because of the limited size of the simulation supercell. At the zone center itself, the LO phonon sets up a uniform electric polarization that is incompatible with the periodic boundary conditions on the supercell.

Cochran and Cowley's expression for the dynamical matrix is

$$\tilde{\phi}_{n,\alpha;p,\beta}(\mathbf{k}) = \tilde{\phi}^{N}_{n,\alpha;p,\beta}(\mathbf{k}) + \frac{4\pi e^2}{\Omega|\mathbf{k}|^2\sqrt{M_n M_p}} \times \left(\sum_{\gamma=1}^{3} k_\gamma Z_{n,\gamma,\alpha}(\mathbf{k})\right)^{*} \epsilon_0^{-1}(\mathbf{k}) \times \left(\sum_{\gamma=1}^{3} k_\gamma Z_{p,\gamma,\beta}(\mathbf{k})\right), \tag{3}$$

where $\mathbf{k}$ is the wave vector, e is the electronic charge, Ω is the volume of the unit cell, M_n is the mass of ion n, $Z_{n,\alpha,\beta}(\mathbf{k})$ is the Born effective charge tensor for ion n, and $\epsilon_0(\mathbf{k})$ is the electronic (frequency-dependent) dielectric function. The first term on the right-hand side is the component of the dynamical matrix that is analytic as $\mathbf{k}\to 0$, while the second term is the nonanalytic part due to macroscopic polarization effects. We use our matrix of force constants evaluated using the Hellmann-Feynman theorem in a cubic supercell to evaluate the analytic part as

$$\tilde{\phi}^{N}_{n,\alpha;p,\beta}(\mathbf{k}) = \frac{1}{\sqrt{M_n M_p}} \sum_{m} \phi_{0,n,\alpha;m,p,\beta} e^{-i\mathbf{k}\cdot(\mathbf{R}_0 - \mathbf{R}_m)}, \tag{4}$$

where $\mathbf{R}_m$ is the position vector of unit cell m.

Following Parlinski *et al.*,[12] we assume that the second term on the right-hand side of Eq. (3) falls off from its value at the Brillouin-zone center with a Gaussian profile. For wave vectors in the first Brillouin zone this term is

$$\frac{4\pi e^2}{\Omega|\mathbf{k}|^2\sqrt{M_n M_p}\,\epsilon_0(\mathbf{0})} \left(\sum_{\gamma=1}^{3} k_\gamma Z_{n,\gamma,\alpha}(\mathbf{0})\right)^{*} \times \left(\sum_{\gamma=1}^{3} k_\gamma Z_{p,\gamma,\beta}(\mathbf{0})\right) \times e^{-(|\mathbf{k}|/\rho_0\kappa^{1/2})^2}, \tag{5}$$

where $\kappa^{1/2}$ is the distance from the center to the boundary of the Brillouin zone along the k_x, k_y, and k_z directions, and ρ_0 is a parameter determining the rate at which the term falls off as the edge of the Brillouin zone is approached. Following Parlinski *et al.*, we set $\rho_0 \equiv 1.2$.

The frequency density-of-states function is evaluated using the method of Swift,[15] in which the Brillouin zone is sampled using Monte Carlo methods. For a single harmonic mode of frequency ω, the Helmholtz free energy is given by

$$F_1(\omega) = k_B T \log(e^{\beta\hbar\omega/2} - e^{-\beta\hbar\omega/2}), \tag{6}$$

where $\hbar$ is the Dirac constant, k_B is Boltzmann's constant, T is the temperature, and $\beta = 1/k_B T$. Hence, by numerically integrating the product of the specific density of states with the mean free energy of a normal mode, the specific lattice

thermal free energy can be calculated for a range of temperatures. The dependence on density is found by interpolating between the results at different lattice parameters. We note that for high symmetry structures, once the phonon eigenvectors are determined at one volume, only a single calculation of restoring forces with all atoms displaced in all directions is required at other volumes, since the displacement pattern can be projected onto frozen phonons.

B. Gibbs free energy

We have calculated the Helmholtz free energy $f(v,T)$ as a function of temperature T and specific volume v (the reciprocal of the density). However, the appropriate thermodynamic potential for constructing the (p,T)-phase diagram and evaluating the polymorphic equation of state is the specific Gibbs free energy $g(p,T)$, where p is the pressure. The Gibbs free energy function for each phase can be evaluated using the Legendre transformation

$$g(p,T)=f+pv=f-\left(\frac{\partial f}{\partial v}\right)_T v. \tag{7}$$

C. Phase diagram

Under conditions of fixed pressure and temperature, the system consists entirely of the available phase with the lowest Gibbs free energy. Thus the phase diagram in (p,T) space can be evaluated.

D. Combining phases

For each pressure and temperature, we may evaluate the polymorphic Gibbs free energy $g_{\rm poly}(p,T)$ as the lowest of the Gibbs free energies for each phase. Given this, we may carry out a Legendre transformation to the polymorphic Helmholtz free energy:

$$f_{\rm poly}(v,T)=g_{\rm poly}-pv=g_{\rm poly}-p\left(\frac{\partial g_{\rm poly}}{\partial p}\right)_T. \tag{8}$$

Differentiating this, we obtain the pressure as a function of specific volume and temperature: the desired polymorphic equation of state.

III. EXTENSION OF THE QUASIHARMONIC METHOD TO UNSTABLE PHONONS

A. Analytic model of soft-mode phonons

In minerals such as perovskites[7] it is possible to describe the transition from a high-temperature phase to a low-temperature phase of lesser symmetry as the ''freezing in'' of a finite amplitude of an unstable phonon of the high-symmetry phase, plus a finite strain on the unit cell. We consider the application of quasiharmonic ideas to these materials.

The simple harmonic model gives a negative energy and a divergent free energy arising from the unstable modes. In reality, the soft-mode phonon is best described by a potential double well with a local maximum at the mean structure, corresponding to the high-symmetry phase.

Let x_i be a coordinate describing the structural feature involved in the phase transition at a particular wave vector. The corresponding normal mode can be modeled by considering the dynamics of the set of $\{x_i\}$ moving in fixed local potential double wells.[16] In the harmonic limit, normal modes are uncoupled. However, because we are considering finite displacements there will in general be coupling between our double-well oscillators, this being most pronounced around the phase transition and at high temperatures. Coupling can be approximately treated by renormalization.[16]

Much work has been concentrated on the Landau model, in which the double-well is a *free energy* in the form of a quartic polynomial $V(x)=Ax^4-B(T)x^2$, where $B(T)$ changes sign with temperature through coupling to other modes. Such a polynomial expansion of the *total energy* is also possible, perhaps incorporating still higher-order terms.[3] However, analytic terms beyond second order imply phonon coupling. This is inconsistent with the harmonic approximation used to describe nonsoft modes: even at a high phonon number the normal modes are assumed to be harmonic and therefore independent of each other.

We propose instead to describe the entire soft-phonon branch via a double well of the form

$$V(x)=\tfrac{1}{2}m\omega_0^2x^2+\epsilon(e^{-x^2/2\sigma^2}-1), \tag{9}$$

where ϵ, ω_0, and σ are wave vector dependent. Provided that $\epsilon>m\omega_0^2\sigma^2$, there are minima at

$$x=x_\pm\equiv\pm\sqrt{2\sigma^2\log(\epsilon/m\omega_0^2\sigma^2)}, \tag{10}$$

separated by a barrier of height

$$\Delta V\equiv V(0)-V(x_\pm)=\epsilon-m\omega_0^2\sigma^2[1+\log(\epsilon/m\omega_0^2\sigma^2)]. \tag{11}$$

This form of potential has the advantage of being approximately quadratic in both the low- and high-energy limits. Specifically, for the low-energy case at $x=x_\pm$, we have

$$\frac{d^2V}{dx^2}=2m\omega_0^2\log(\epsilon/m\omega_0^2\sigma^2), \tag{12}$$

which is equivalent to a harmonic oscillator of frequency

$$\omega_0'=\sqrt{2\omega_0^2\log(\epsilon/m\omega_0^2\sigma^2)}. \tag{13}$$

On the other hand, for the high-energy case, the potential approximates that of an harmonic oscillator of frequency ω_0.

Soft modes do not usually show an abnormal dependence on temperature—except in the vicinity of the phase transition. Therefore, we expect our model to be more widely applicable than models where soft modes are treated as quartic and other modes as harmonic.

The (imaginary) harmonic frequency ω_c about the (unstable) center of the well is given by

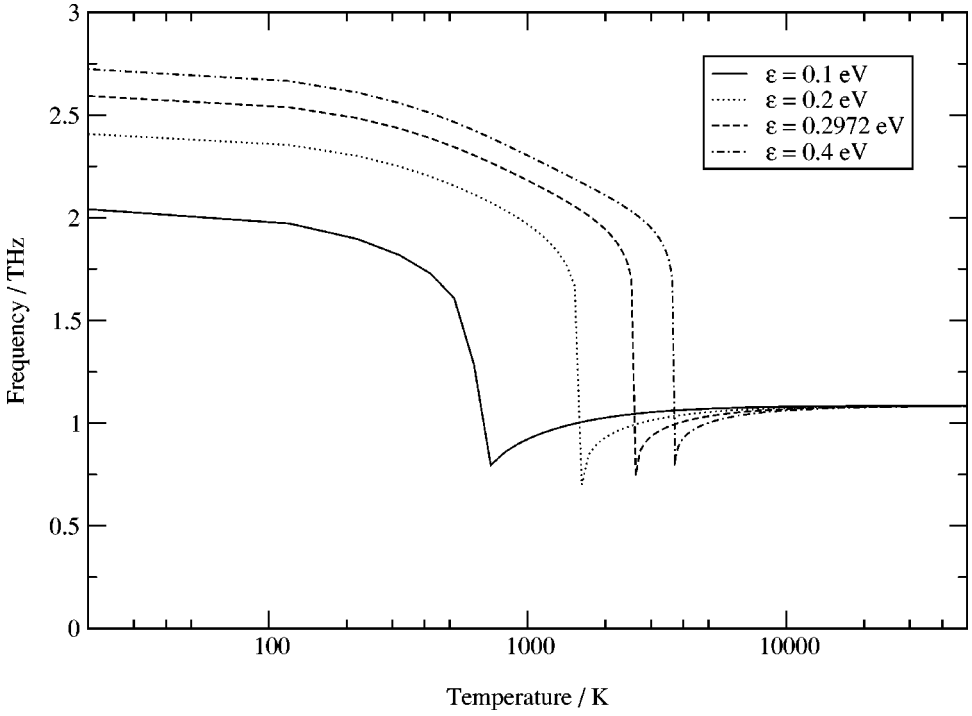

FIG. 1. Classical frequency of a double-well oscillator in thermal contact with a heat bath plotted against temperature for various barrier heights ϵ. The other double-well parameters are $m=1$, $\omega_0=0.0691$ $\mathrm{eV}^{1/2}\,\mathrm{Å}^{-1}\,\mathrm{amu}^{-1/2}$, and $\sigma=1.866$ $\mathrm{amu}^{1/2}\,\mathrm{Å}$. The frequency falls to zero in a cusp at the phase transition. At $\epsilon=0.2972$ eV, the double-well parameters are appropriate for the double-well describing the orthorhombic-tetragonal transition in $MgSiO_3$ at zero pressure (Ref. 7). Thus this model predicts a soft mode transition temperature of 2609 K, if the coupling of the soft phonon to strain is neglected.

$$\omega_c^2=\omega_0^2-\frac{\epsilon}{m\sigma^2}. \tag{14}$$

B. Isolated double-well oscillators

We now consider the problem of motion in an isolated potential double well.

1. Classical solution

To evaluate the mechanical energy, we assume that the mode is in thermal contact with a heat bath at the appropriate temperature. The mean energy is given by

$$\langle E\rangle=\frac{\int_{-\infty}^{\infty}\int_{-\infty}^{\infty}H(p,x)e^{-\beta H(p,x)}dp\,dx}{\int_{-\infty}^{\infty}\int_{-\infty}^{\infty}e^{-\beta H(p,x)}dp\,dx}$$

$$=\frac{k_BT}{2}+\frac{\int_0^{\infty}V(\sigma z)e^{-\beta V(\sigma z)}dz}{\int_0^{\infty}e^{-\beta V(\sigma z)}dz}, \tag{15}$$

where $H(p,x)=p^2/2m+V(x)$ is the Hamiltonian of the isolated mode as a function of x and p, the canonical momentum conjugate to x. $\beta=1/k_BT$ where k_B is Boltzmann's constant and T is the temperature.

For a given energy E, the frequency of our isolated mode can be evaluated using the action-angle method. The action variable is

$$j\equiv\frac{1}{2\pi}\oint p\,dx. \tag{16}$$

If the mode has an energy $E\geqslant\epsilon$, so that there is sufficient energy to cross the barrier, each libration, we find that

$$j=\frac{2\sigma}{\pi}\int_0^{x_M(E)/\sigma}\sqrt{2mE-m^2\omega_0^2\sigma^2z^2-2m\epsilon e^{-z^2/2}}dz, \tag{17}$$

where x_M is the positive solution of $V(x)=E$. On the other hand, if $E<\epsilon$, so that the motion is confined to one side of the double well, we find that

$$j=\frac{\sigma}{\pi}\int_{x_m(E)/\sigma}^{x_M(E)/\sigma}\sqrt{2mE-m^2\omega_0^2\sigma^2z^2-2m\epsilon e^{-z^2/2}}dz, \tag{18}$$

where x_M is the greater of the two positive solutions and x_m is the lesser.

In either case, the corresponding frequency ω may be evaluated using Eq. (19):

$$\frac{1}{\omega}=\frac{\partial j}{\partial E}. \tag{19}$$

Taken together, the results of Eqs. (15), (17), (18), and (19) allow us to calculate numerically the frequency of an isolated oscillator moving with the mean thermal energy as a function of temperature. Example results are shown in Fig. 1. A typical ''soft-mode'' behavior is observed, with the frequency dropping to zero in a cusp at the transition temperature. This simple approach was used in early studies of $MgSiO_3$.[17]

2. Quantum solution

The energy eigenfunctions of a particle moving in a symmetric potential must be either symmetric or antisymmetric.

Furthermore, by considering building up the Gaussian barrier adiabatically, it is clear that the symmetry of the eigenfunctions must be the same as for those of the harmonic oscillator.

The definite symmetry of the wavefunctions leads to a ''paradox'' for wells of finite separation. If we know the energy of the oscillator then it is in an energy eigenstate and the wave function is either symmetric or antisymmetric. Hence the probability distribution is symmetric about the center of the double well, and we cannot meaningfully say which side the oscillator is confined in, even if its energy is much less than the barrier height. Thus it is not conceptually clear that equating the mean thermal energy with the barrier height gives the correct transition temperature. We discuss this further in Sec. III D.

The Hamiltonian operator for a particle moving in the quadratic potential *without* the additional Gaussian potential is

$$\hat{H}^0 = -\frac{\hbar^2}{2m}\frac{\partial^2}{\partial x^2} + \frac{1}{2}m\omega_0^2 x^2. \tag{20}$$

The well-known energy eigenvalues and eigenfunctions for the time-independent Schrödinger equation $\hat{H}^0\phi_n = E_n^0\phi_n$ are

$$E_n^0 = (n+1/2)\hbar\omega_0 \tag{21}$$

and

$$\phi_n = \frac{2^{-n/2}}{\sqrt{n!}}\left(\frac{m\omega_0}{\hbar\pi}\right)^{1/4} e^{-m\omega_0 x^2/2\hbar} H_n\left(\sqrt{\frac{m\omega_0}{\hbar}}x\right) \tag{22}$$

for $n \in \mathcal{N}_0$, where $H_n(x)$ is the nth Hermite polynomial.

The Hamiltonian operator for a particle moving in the double well is $\hat{H} = \hat{H}^0 + V_1$, where $V_1 = \epsilon(e^{-x^2/2\sigma^2} - 1)$ is the extra Gaussian term. Let the eigenfunctions and eigenenergies of the full Hamiltonian be ψ_n and E_n.

The eigenfunctions of the simple harmonic oscillator (SHO) are chosen as the basis of wave-function space. This choice makes the computation particularly simple, as will be seen below.

The matrix elements of the Hamiltonian with respect to our chosen basis are

$$\langle\phi_i|\hat{H}\phi_j\rangle = \langle\phi_i|\hat{H}^0\phi_j\rangle + \langle\phi_i|V_1\phi_j\rangle = (i+1/2)\hbar\omega_0\delta_{i,j} + \frac{\epsilon}{2^{(i+j)/2}\sqrt{i!j!\pi}}\int_{-\infty}^{\infty} e^{-Kz^2}H_i(z)H_j(z)dz, \tag{23}$$

where $K \equiv \hbar/2m\omega_0\sigma^2 + 1$. Note that the matrix is real and symmetric.

The Hermite polynomials satisfy $H_i(-x) = (-1)^i H_i(x)$, so that $\langle\phi_i|V_1\phi_j\rangle = 0$ if $i+j$ is odd. If $i+j$ is even then the integrand is an even function. Hence, in this case,

$$\langle\phi_i|V_1\phi_j\rangle = \frac{2\epsilon}{2^{(i+j)/2}\sqrt{i!j!\pi}}\int_0^{\infty} e^{-Kz^2}H_i(z)H_j(z)dz. \tag{24}$$

The eigenvalues of the matrix of the Hamiltonian are the allowed energy levels. For energies that are large compared with the barrier height the particle will spend most of its time away from the center of the well; hence we expect that the system will behave as a SHO in this limit. Indeed, it is clear from Eq. (24) that the elements of the matrix $\langle\phi_i|V_1\phi_j\rangle$ fall off rapidly as i and j increase. Hence, for large i or j, the eigenstates of the Hamiltonian tend to to those of the SHO. Thus we only need to diagonalize the upper left-hand corner [say, the $(n_c+1)\times(n_c+1)$ submatrix] in order to obtain the first n_c+1 energy levels E_0 to E_{n_c}. Beyond n_c the eigenstates may be taken to be those of the SHO. The comparative ease with which the Hamiltonian matrix can be diagonalized is one of the advantages of the quadratic-plus-Gaussian double-well potential over the quartic double-well potential, although there is no analytic form equivalent to Eq. (6).

Assuming that n_c is sufficiently large, the canonical partition function can be written as

$$Z = \sum_{n=0}^{n_c} e^{-\beta E_n} + \sum_{n=n_c+1}^{\infty} e^{-\beta(n+1/2)\hbar\omega_0} = \sum_{n=0}^{n_c} e^{-\beta E_n} + \frac{e^{-\beta\hbar\omega_0(n_c+1)}}{e^{\beta\hbar\omega_0/2} - e^{-\beta\hbar\omega_0/2}}. \tag{25}$$

The free energy of the double-well oscillator can then be evaluated as

$$F_1 = -k_B T \log(Z). \tag{26}$$

C. Practical implementation in the quasiharmonic method

Having proposed that each soft mode at a given wave vector be described by a double well of the form given in Eq. (9), we now describe how the parameters ϵ, σ, and ω_0 can be determined. Note that if $\{x_i\}$ are mass-reduced phonon coefficients then we may, without loss of generality, set $m=1$.

Consider the phonon dispersion curve of a crystal structure in which imaginary frequencies are present. Those branches that remain real throughout the whole of the Brillouin zone are treated as harmonic and, for each mode at each wave vector, Equation (6) may be used to find the corresponding free energy. For those branches that are imaginary in some region of the Brillouin zone, however, we propose the following treatment.

(1) At each symmetry point of the Brillouin zone the eigenvector corresponding to the relevant mode should be evaluated and the displacement pattern frozen into the crystal. *Ab initio* techniques can then be used to find the corresponding low-symmetry structure, if desired. Using three total-energy calculations with different amplitudes of the soft phonon frozen into the structure,[34] we may evaluate the parameters ϵ, σ and ω_0 of the double well. Note that it is

possible to fit Eq. (9) to every branch even if the mode is not imaginary since that Eq. (9) does not necessarily describe a double well. In practice the harmonic approximation is used for all-real branches, it is equivalent to setting $\epsilon=0$.

(2) For each branch we use our results for the double-well parameters at the symmetry points to construct interpolating polynomials over the whole of the Brillouin zone for the ϵ and σ parameters.

(3) For any wave vector in the Brillouin zone, we may find the spectrum of corresponding (possibly imaginary) frequencies. Provided we know to which branch these modes belong, we have sufficient information to determine the parameters of the appropriate double-well for each mode. ϵ and σ are found by interpolating to our wavevector and the unstable frequency gives ω_c [see Eq. (14)], from which we may find $\omega_0^2=\omega_c^2+\epsilon/m\sigma^2$.

(4) Hence, for any given wave vector, the free energy of each mode, whether harmonic or soft, can be evaluated. These free energies can be summed to give the free-energy contribution from all modes at the given wavevector.

(5) The free energy can then be integrated over all wave vectors in the Brillouin zone to give the total lattice thermal free energy. By using a grid-based scheme to integrate over an irreducible wedge of the zone and by making use of the continuity of the gradient of each branch, it is possible to keep track of which branch is which—necessary if the appropriate values of ϵ and σ are to be interpolated in the pressence of imaginary branch crossings. The problem of interpolation over an irreducible wedge of the Brillouin zone has been studied extensively in the context of electronic eigenvalues: see, for example, Ref. 18.

The high-symmetry dynamically stabilized phase and the low-symmetry ''frozen-phonon'' phase can now be treated as being distinct. Hence the methodology of Sec. II B can be applied to find the phase diagram.

D. Interpretation of the soft mode transition

Consider an isolated symmetric double-well oscillator. For the probability density to be asymmetric—necessary if we are to meaningfully say that the particle is in one well or the other—we must have a mixture of symmetric and antisymmetric energy eigenstates. Therefore, we cannot simultaneously know the energy of our particle *and* which well it is in unless we break the symmetry (e.g., by allowing the crystal to distort under phonon-strain coupling).

If the oscillating particle's wave function is a superposition of different energy eigenfunctions then the expansion coefficients will evolve in time (provided the system remains both undisturbed *and* unobserved) according to the Schrödinger equation. Hence the quantum mechanical expectation value of the particle's position $\langle x\rangle$ changes in time.

The time-dependent wave function can be written as

$$\Psi(x,t)=\sum_{n=0}^{\infty} c_n e^{-iE_n t/\hbar}\psi_n(x). \tag{27}$$

Hence the expectation of x can be written as

$$\langle x\rangle=\sum_{n=0}^{\infty}\sum_{m=0}^{\infty} c_n^* c_m e^{i(E_n-E_m)t/\hbar}\langle\psi_n|x\psi_m\rangle$$

$$=2\sum_{n\ \mathrm{even}}\sum_{m\ \mathrm{odd}}|c_n||c_m|\cos(\omega_{nm}t+\eta_{nm})\langle\psi_n|x\psi_m\rangle, \tag{28}$$

where $\omega_{nm}=|E_n-E_m|/\hbar$ and $\eta_{nm}=[\arg(c_m)-\arg(c_n)]\mathrm{sgn}(\omega_{nm})$. Note that we use the fact that $\langle\psi_n|x\psi_m\rangle=0$ if ψ_n and ψ_m are either both odd or both even, since x itself is odd. We also use the fact that $\langle\psi_n|x\psi_m\rangle=\langle\psi_m|x\psi_n\rangle$.

We assume that the energy levels are initially populated according to Boltzmann statistics; thus $|c_n|^2=Z^{-1}e^{-\beta E_n}$, where $\beta=1/k_BT$ and $Z=\Sigma_{n=0}^{\infty}e^{-\beta E_n}$ is the canonical partition function. So we have

$$\langle x\rangle=\sum_{n\ \mathrm{even}}\sum_{m\ \mathrm{odd}}\Gamma_{nm}\cos(\omega_{nm}t+\eta_{nm}), \tag{29}$$

where $\Gamma_{nm}=2Z^{-1}e^{-\beta(E_n+E_m)/2}\langle\psi_n|x\psi_m\rangle$ is the amplitude of the sinusoidal component in the expansion of $\langle x\rangle$ with frequency ω_{nm}.

For the harmonic-oscillator potential, the frequencies of the oscillations in $\langle x\rangle$ are of the form $\omega_{nm}=|E_n-E_m|/\hbar=|n-m|\omega_0$. Thus the lowest oscillation frequency is ω_0. For the symmetric double well, however, we end up with a set of pairs of energy levels that are very close to each other (becoming degenerate in the limit that the barrier height goes to infinity). These give rise to oscillation frequencies very much lower than ω_0.

As the temperature is increased, higher-frequency components have larger Γ coefficients. We suggest that the soft-mode phase transition be judged to occur when the frequency with the highest coefficient exceeds the frequency of the experimental probe. When this has happened, the predominant sinusoidal component of $\langle x\rangle$ has a frequency higher than can be measured by the experimental probe, and so it appears to the experimenter that $\langle x\rangle=0$. Below this temperature, measurements of $\langle x\rangle$ will tend to find it in one well or the other. This definition is different from the polymorphic one (Sec. II B) because of the contribution to the free energy from the symmetry-breaking distortion of the lattice that inevitably accompanies the transition. In particular, the quasiharmonic transition is first-order while this measurement dependent ''soft-mode'' one is second order.[16]

Thus the first-order transition is determined by comparing (1) the free energy of the soft-mode phase, calculated as above, expanded about an unstable frozen-ion structure without strain-phonon coupling, with (2) the free energy of the low symmetry phase, calculated by expanding about the minimum of total energy. Typically, the former will have a higher entropy (sampling from both wells), while the latter has a lower energy.

E. Absorption of low-frequency photons

Figure 2 shows the energy difference between neighboring energy levels $(E_n-E_{n-1})/\hbar$ plotted against the mean of

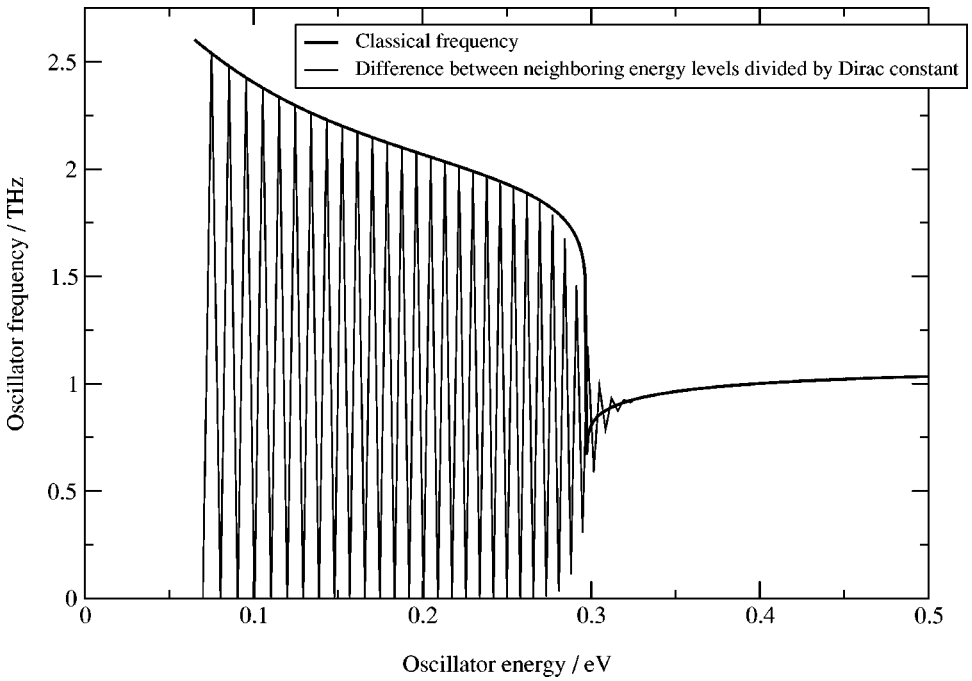

FIG. 2. Thick line: frequency of a classical isolated double-well oscillator against energy. The double-well parameters are as in Fig. 1 with $\epsilon = 0.2972$ eV. Fine line: energy differences $(E_i - E_{i-1})/\hbar$ against energy $(E_i + E_{i-1})/2\hbar$ for a quantum oscillator.

the two energies $(E_n + E_{n-1})/2$ for the quantum double-well oscillator. Absorption of photons at frequency $(E_n - E_{n-1})/\hbar$ is symmetry allowed.

For energies in excess of the barrier height the frequency $(E_n - E_{n-1})/\hbar$ is virtually identical to the classical frequency for energy $(E_n + E_{n-1})/2$, obtained using the method of Sec. III B 1. In the very high-energy limit the frequency behaves as that of the quadratic potential well without the Gaussian barrier.

For energies less than the barrier height the energy levels tend to degenerate pairs of levels. The frequencies given by the difference between the energy levels of neighboring pairs again correspond to the classical frequencies. However, the pairs of almost-degenerate eigenstates imply the existence of very low-frequency absorption peaks. (These are the very low frequencies that alternate with the classical frequencies below the transition energy in Fig. 2.) It should be noted that these frequencies are not associated with the normal modes of the low-symmetry phase and do not, therefore, contribute to the quasiharmonic thermal energy. They are a feature of the quantum double-well oscillator without a classical analog.

IV. APPLICATION OF QUASIHARMONIC METHODS TO PERICLASE

A. Computational details

1. Cold curve

For each lattice parameter the total energy is evaluated using the CASTEP software package,[19] which utilizes density-functional theory in the generalized gradient approximation (GGA).[20] The ionic cores are accounted for using ultrasoft pseudopotentials[21] in Kleinman-Bylander form.[22] The wave functions of the valence electrons are expanded in a plane-wave basis set up to an energy cutoff of 540 eV.

For the $B1$ phase, the simulation cell consists of a single cubic unit cell. The Brillouin zone is sampled at 20 special points generated from an $8\times8\times8$ mesh using the Monkhorst-Pack scheme.[23] For the $B2$ phase, the simulation cell is a single cubic primitive cell. The Brillouin zone is sampled at 35 special points from a $9\times9\times9$ mesh. In each case the point symmetries of the crystal are enforced.[24]

The equilibrium lattice parameter of the $B1$ phase at zero external pressure (which corresponds to the minimum of the cold-curve) calculated using CASTEP is $a = 4.259$ Å, which may be compared with an experimentally determined parameter $a = 4.2115(1)$ Å.[28] The difference between the theoretical and experimental values is about 1%.

2. Determination of the matrix of force constants

The supercells simulated to determine the matrices of force constants for the $B1$ phase consist of $2\times2\times2$ cubic unit cells (64 atoms). Thus the interactions between a given ion and its third-closest shell of neighbors are included in our calculations. For the $B2$ phase, the cells used consist of $2\times2\times2$ cubic primitive unit cells (16 atoms). In these supercells the crystal symmetry is such that only two ionic displacements are required to complete the entire matrix of force constants. The plane-wave cutoff energy is 540 eV and the Brillouin zone is sampled at six special points from a $4\times4\times4$ mesh. In each simulation the ion displaced from equilibrium is moved by 0.4% of the lattice parameter.

As demonstrated by Parlinski *et al.*,[12] it is possible to calculate the Born effective charge tensors from first principles using simulations of elongated supercells. Note that because of the symmetry of the $B1$ and $B2$ phases, the Born effective charge tensors are isotropic (so $Z_{n,\alpha,\beta} = Z_n \delta_{\alpha,\beta}$). Furthermore, the sum of the Born effective charges over the ions in a unit cell must be zero[14] (so $Z_{\mathrm{Mg}} = -Z_{\mathrm{O}}$). Hence there is

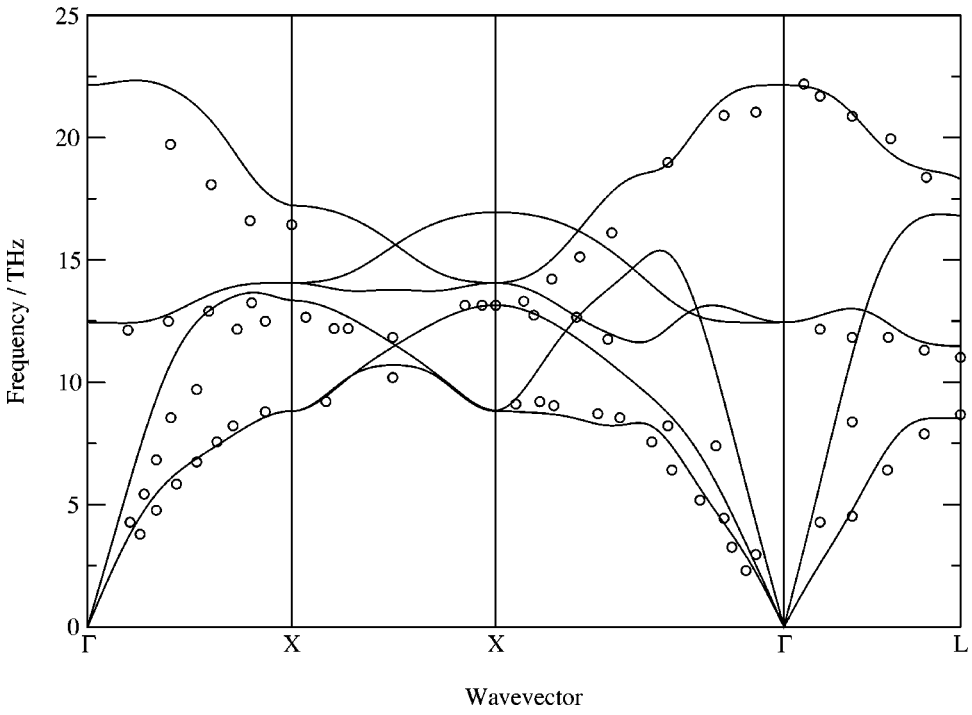

FIG. 3. Dispersion curves for $B1$ MgO at a lattice parameter 4.2 Å. The symmetry points in the dispersion curve are (from left to right) Γ [000], X [001], X [011], Γ [000], and L $[\frac{1}{2}\frac{1}{2}\frac{1}{2}]$. Note the LO-TO splitting (at Γ, the LO frequency is 22.0 THz whereas the TO frequency is 12.4 THz) arising from the nonanalytic term of Eq. (5). Also shown are Peckham's experimental results for $B1$ MgO at a lattice parameter 4.212 Å. Note that the reciprocal-lattice vectors referred to in the results for the $B1$ phase are those of the cubic unit cell rather than the true reciprocal-lattice vectors.

effectively only one undetermined parameter in the nonanalytic term: $Z_{\mathrm{Mg}}(\mathbf{0})/\sqrt{\epsilon_0(\mathbf{0})}$.

We choose $Z_{\mathrm{Mg}}(\mathbf{0})/\sqrt{\epsilon_0(\mathbf{0})}=4.4$ to give the LO branch in the dispersion curve of Fig. 3. Our values for the effective charge tensors of the $B1$ phase are such that the calculated LO branch for lattice parameter 4.2 Å are in reasonable agreement the experimental results of Peckham.[25] We neglect the variation of the effective charge tensors with lattice parameter.

B. Approximations and errors

1. Errors in ab initio total-energy calculations

Total-energy differences between structures calculated using density-functional theory in the generalized gradient approximation are thought to be reliable to within a few percent.[22] The cutoff energy of the plane-wave basis at 540 eV is sufficient for convergence of the total energies of the crystals to within 10 μeV per ion, several orders of magnitude less than the likely error due to the use of the GGA. The Hellmann-Feynman forces are converged to within 1 meV $\mathrm{Å}^{-1}$, at least two orders of magnitude less than the dominant forces arising when an ion is displaced.

2. Harmonic approximation

We investigate the range of validity of the harmonic approximation. This is done for the $B1$ phase with a lattice parameter $a=4.2$ Å.

We evaluate the force constant of the restoring force on a magnesium ion as it is displaced in the x direction. The results are shown in Fig. 4. It can be seen that the force constant starts to increase when the ionic displacement reaches $a_{\max}\approx 0.084$ Å, about 2% of the lattice parameter, at which point the potential energy is about 0.4 eV. Other displacements are similar; hence it is reasonable to assume that the forces remain linear (and the quasiharmonic assumption is valid) for temperatures up to several thousand K.

3. Other sources of error

Another potential source of error is the limited size of the simulation supercells. However, the results shown in Table I for the $B1$ phase make it clear that interactions beyond the third-closest shell of neighbors may be safely neglected.[26] Contributions to the free energy from the thermal excitation of the valence electrons, from coupled electron-phonon excitations and from the equilibrium population of defects are thought to be negligible in comparison with the frozen-ion and lattice thermal energies.[15]

A poor convergence of the Hellmann-Feynman forces can result in the violation of Newton's third law for the matrix of force constants. Typically this results in the acoustic branches of the dispersion curve failing to pass through zero at the center of the Brillouin zone.[11] As discussed in Sec. II A 2, Newton's third law is imposed on the matrix of force constants. However, even without this, the calculated acoustic branches pass very close to zero at the zone center.

The method by which long-range polarization effects are accounted for is also approximate. The effects of this are discussed below.

C. *Ab initio* phonons

1. B1 phase

Inelastic neutron-scattering experiments were carried out by Peckham,[25] and used to generate dispersion curves for the $B1$ phase.[27] We compare our theoretical dispersion curve with these results in Fig. 3. (Note that our dispersion curve was generated for a lattice parameter of 4.2 Å, whereas Peck-

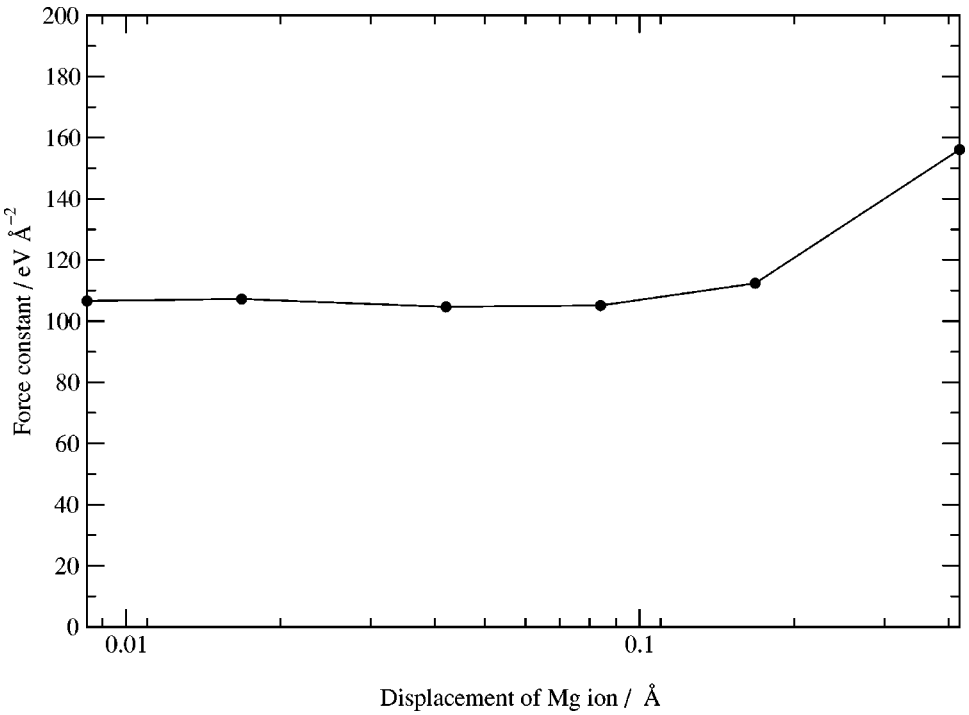

FIG. 4. Graph of the restoring force divided by the finite displacement of a Mg ion in the [100] direction against that displacement. Results are appropriate for a $2\times1\times1$ supercell of the $B1$ phase at a lattice parameter 4.2 Å. The force constant is independent of the magnitude of the displacement until the displacement is at least 0.084 Å. Thereafter the restoring force increases faster than linearly with the displacement; the harmonic approximation has broken down.

ham's results were obtained under ambient conditions where the lattice parameter is 4.212 Å.) Our theoretical results are in reasonable agreement with experiment. (The lattice parameter of 4.2 Å corresponds to a pressure of about 7 GPa at zero temperature.)

The specific frequency density-of-states function is shown in Fig. 5. Without the addition of the nonanalytic term to the dynamical matrix, the longitudinal optic branch is degenerate with the transverse optic branch at the Γ point, and this is also shown. Although only the LO branch is altered substantially, it can be seen that the inclusion of the nonanalytic term has a significant effect on the density of states.

We compare sound velocities calculated from our dispersion curves with the experimental results of Reichmann *et al.*[28] obtained using ultrasonic interferometry. Reichmann *et al.* obtained a *P*-wave sound speed of 9119 ms^{-1} in the [100] direction, whereas our longitudinal-acoustic mode has $(d\omega_{\mathrm{LA}}/dk_{[100]})_{\mathbf{k}=0}=11367\ \mathrm{ms}^{-1}$. On the other hand, in the [111] direction, the experimental *P*-wave velocity is 10125 ms^{-1}, which may be compared with our theoretical value of 10818 ms^{-1}.

TABLE I. Magnitude of the component of force in the [001] direction when the Mg ion at (0,0,0) is displaced in the [001] direction by 0.05% of the length of a $1/\sqrt{2}\times1/\sqrt{2}\times8$ supercell. Coordinates are given as fractions of the supercell dimensions. (These results are for $B1$ MgO at a lattice parameter 4.2 Å.)

Position of Mg atom	Magnitude of [001] component of force / eV Å^{-1}
(0,0,0)	0.13424
(0.5,0.5,0.0625)	0.03356
(0,0,0.125)	0.00981
(0.5,0.5,0.1875)	0.00006

Thus Reichmann *et al.*'s experimental results show a higher degree of anisotropy than do our theoretical results. The discrepancy would appear to be (at least partly) caused by the imposition of symmetry and Newton's third law on the matrix of force constants:[11] if this procedure is not carried out then we find that $(d\omega_{\mathrm{LA}}/dk_{[100]})_{\mathbf{k}=0}=10770\ \mathrm{ms}^{-1}$ and $(d\omega_{\mathrm{LA}}/dk_{[111]})_{\mathbf{k}=0}=12651\ \mathrm{ms}^{-1}$. Although Reichmann *et al.*'s *P*-wave velocities are still somewhat less than these theoretical velocities, both are now in agreement that the velocity in the [100] direction is less than the velocity in the [111] direction.

2. B2 phase

Typical dispersion curves for the $B2$ phase at lattice parameters 2.0 and 2.7 Å are shown in Figs. 6 and 7. At zero temperature these lattice parameters correspond to pressures of 653 GPa and -6 GPa, respectively.

Note the presence of unstable modes at low pressures in the dispersion curve of the $B2$ phase (Fig. 7). We find that the $B2$ phase is structurally unstable for pressures below about 82 GPa. In our calculations for the phase boundary in periclase we do *not* require our method for dealing with soft modes, because the imaginary frequencies are only found in the $B2$ phase at pressures for which the $B1$ phase is clearly favored.

D. *Ab initio* equation of state

We plot the pressure against specific volume for a range of temperatures in Fig. 8. This is the desired thermodynamic equation of state for periclase. Also shown is a third-order Birch-Murnaghan equation of state generated from the isothermal bulk modulus and its first derivative with respect to volume, which were obtained by means of ultrasonic sound velocity measurement.[29]

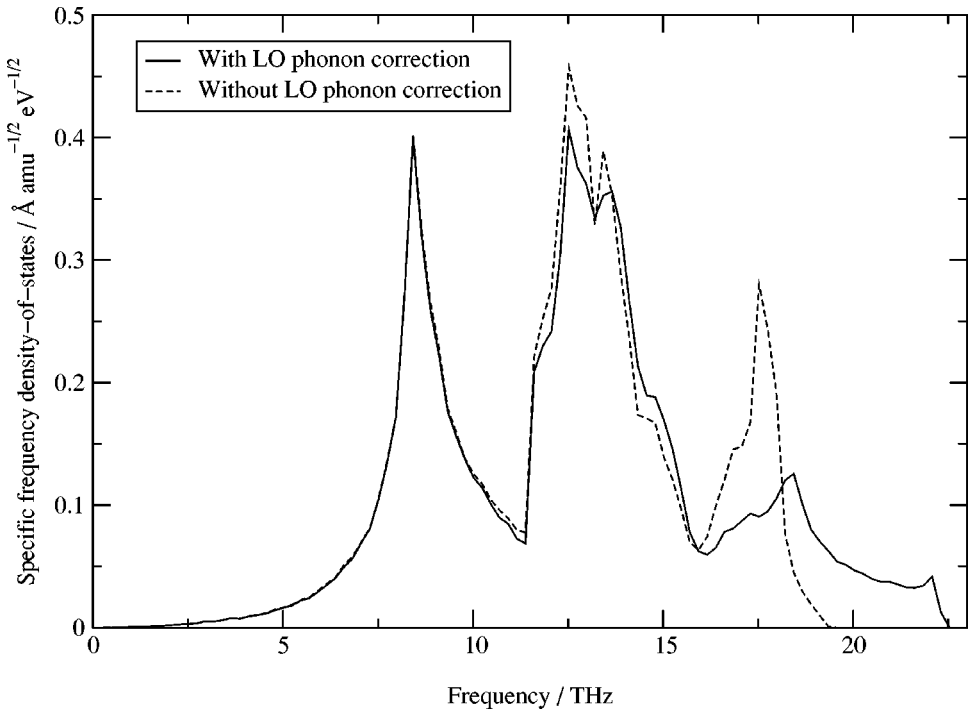

FIG. 5. Specific frequency density of states for the $B1$ phase at a lattice parameter 4.2 Å with and without the inclusion of the nonanalytic term in the dynamical matrix.

As a test of the validity of our results, the isothermal bulk modulus at zero temperature and external pressure (where periclase is entirely in the $B1$ phase) can be compared with experimental results. We calculate the bulk modulus to be $-v(\partial p/\partial v)_{T,v}=155$ GPa, whereas an experimentally determined value is 160.3 ± 0.3 GPa.[29] The theoretical and experimental results differ by about 3%.

We may also compare the pressure derivative of the bulk modulus at zero pressure and temperature with experimental results. The bulk modulus is found to be almost, but not quite, a linear function of pressure. Fitting a straight line to the data from -8.3 to 21.12 GPa we find that the the gradient is 4.11, in excellent agreement with the experimentally determined value of 4.2 ± 0.2.[29] It is found that the pressure derivative of the bulk modulus decreases slightly as the pressure is increased.

E. *Ab initio* phase diagram

The theoretical phase diagram of solid periclase is shown in Fig. 9. At pressures and temperatures below and to the left of the phase boundary shown in the diagram, periclase exists in the $B1$ phase; above and to the right of the boundary it

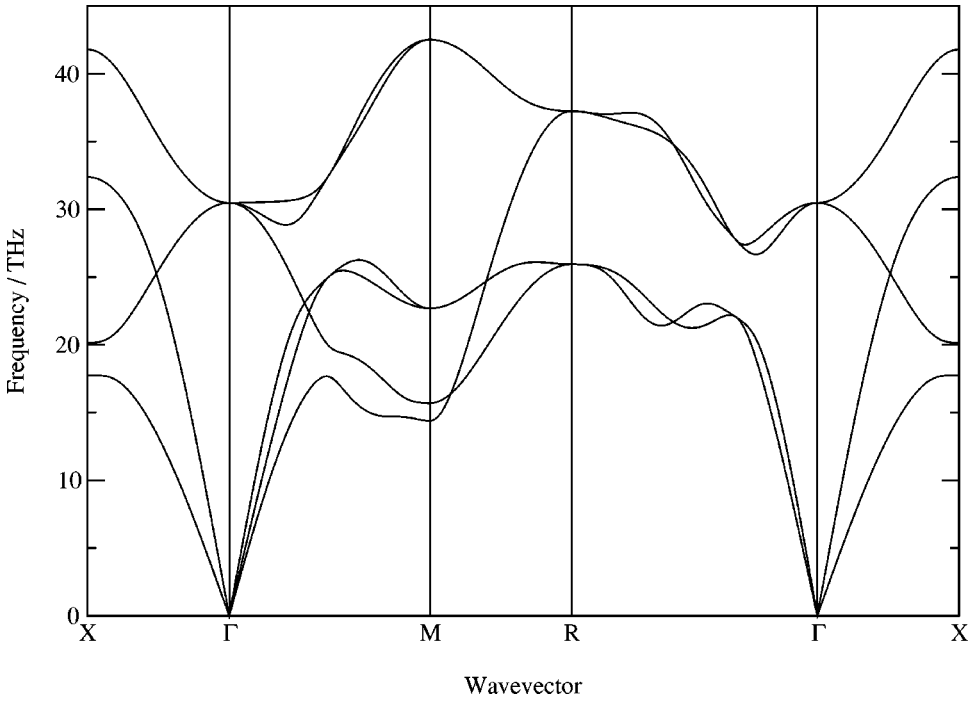

FIG. 6. Dispersion curves for $B2$ MgO at a lattice parameter 2.0 Å. The symmetry points in the dispersion curve are (from left to right) X $[\frac{1}{2}00]$, Γ [000], M $[\frac{1}{2}\frac{1}{2}0]$, R $[\frac{1}{2}\frac{1}{2}\frac{1}{2}]$, Γ [000], and X $[\frac{1}{2}00]$.

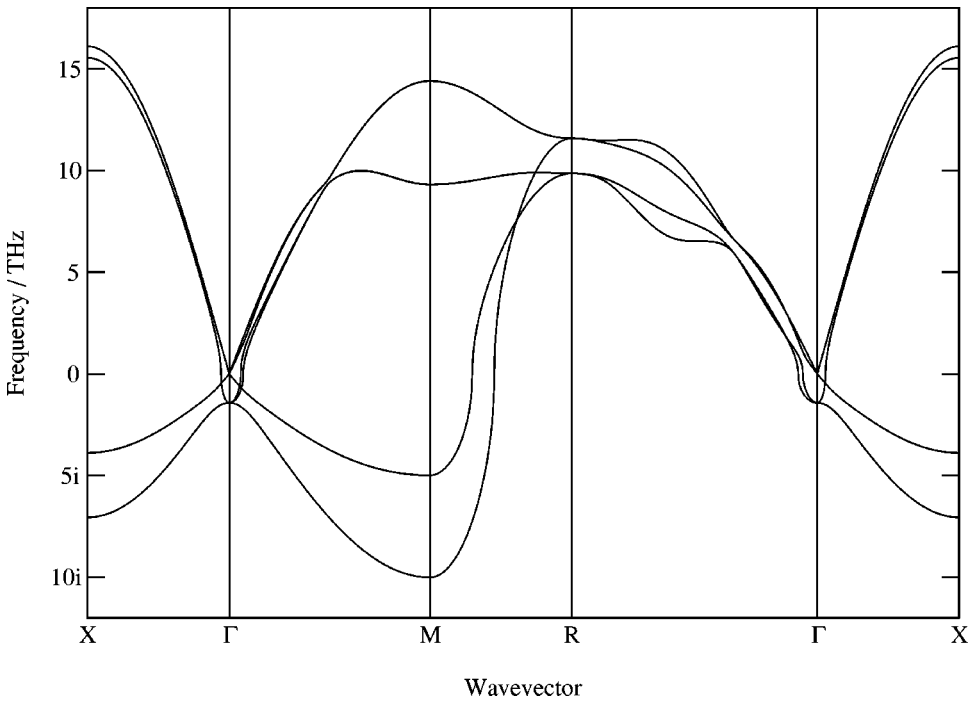

FIG. 7. Dispersion curves for $B2$ MgO at a lattice constant of 2.7 Å. The symmetry points are as in Fig. 6. Note the branches of imaginary phonon frequencies, indicating that the structure is mechanically unstable at this volume.

exists in the $B2$ phase. Duffy *et al.*[30] showed experimentally that, at room temperature, the $B1$ phase is stable to pressures of at least 227 GPa. This lies well within the $B1$ region of our theoretical phase diagram. It can also be noted that the $B2$ phase is not favored at the pressures at which it is structurally unstable.

Also shown in Fig. 9 is the theoretical phase diagram obtained by Strachan *et al.*[31] using a molecular-dynamics simulation. Although qualitatively similar, the calculated position and orientation of the $B1$-$B2$ phase boundary is very different. Karki *et al.*[5] obtained a $B1$-$B2$ transition pressure of 460 GPa at 0 K, which also differs substantially from that of Strachan *et al*. Figure 10 shows the Gibbs free energy plotted against pressure for the two phases at two different temperatures. The difficulty in ascertaining the transition pressures at which the curves cross is apparent. This consideration will affect all theoretical calculations of the phase diagram of periclase.

We confirm the difficulty in locating the transition by attempting to reproduce Karki *et al.*'s zero-temperature results,

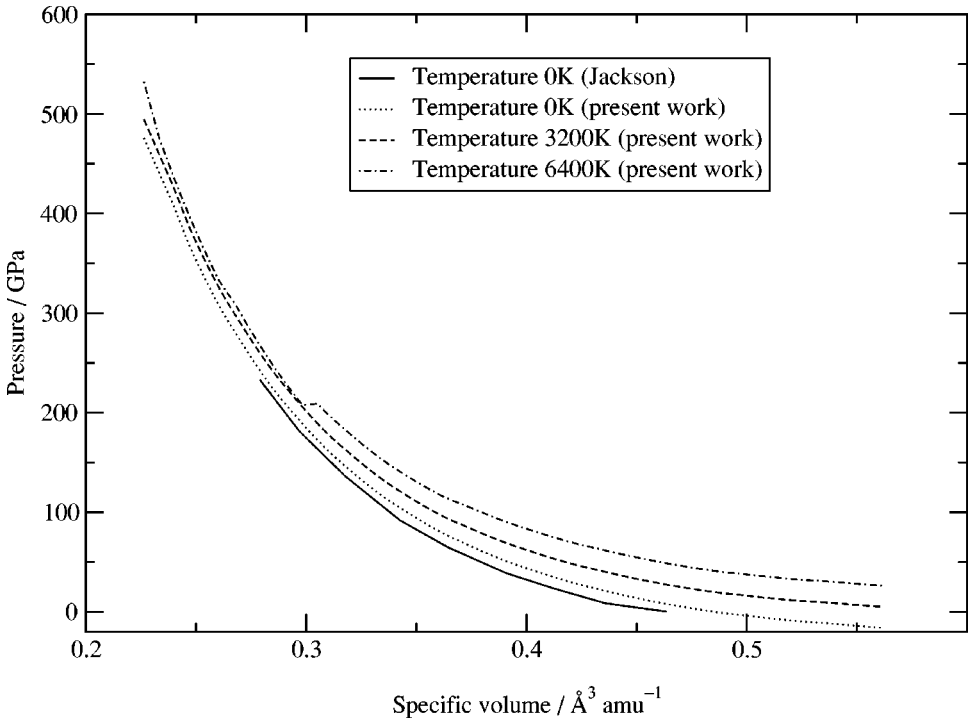

FIG. 8. Equation of state of periclase: pressure against specific volume at various temperatures. The position of the phase transition is clearly visible as a kink in the curves. A Birch-Murnaghan equation of state generated from Jackson's experimental results is also shown.

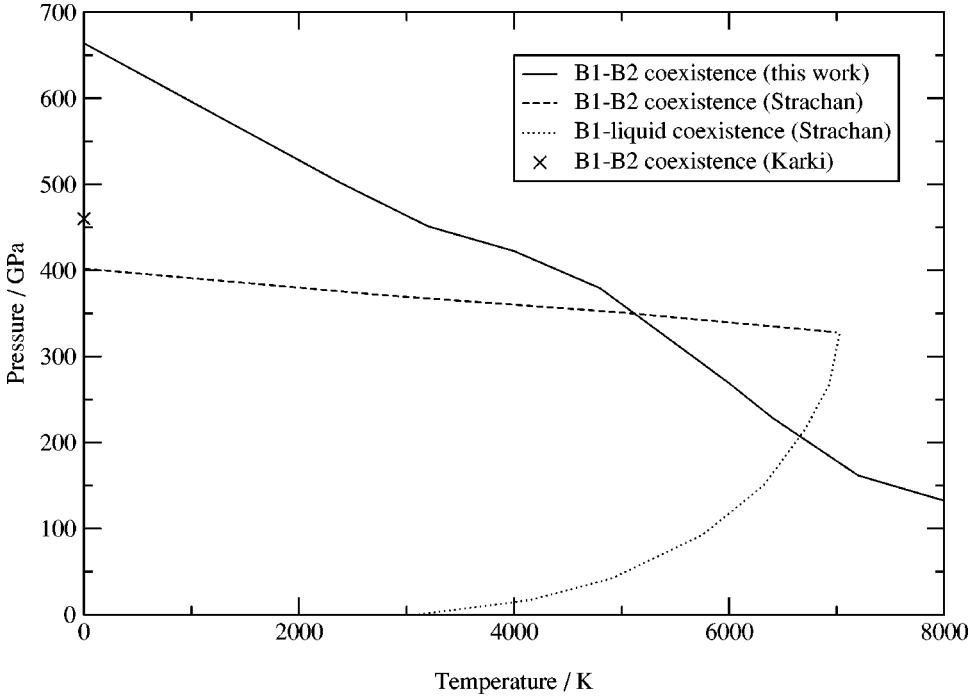

FIG. 9. Theoretical phase diagram of periclase. The $B1$ phase region is below and to the left of the $B1$-$B2$ coexistence line. Also shown are other theoretical results (Refs. 5 and 31), including a theoretical $B1$-liquid phase boundary.

in which zero-point lattice vibrational energy is neglected. We simply calculate the enthalpy against pressure for the two phases using CASTEP. The results are shown in Fig. 11. We find a transition pressure of 664 GPa, different from that of Karki *et al.* (460 GPa). The possibility of a metallization transition lowering the energy of the $B2$ phase was investigated but found not to occur at relevant pressures.

We consider the fractional error in unit-cell volume for the $B2$ phase to which the difference between the specific enthalpies of the $B1$ and $B2$ phases at 451 GPa corresponds. For a given unit-cell enthalpy for the $B2$ phase, we find the fractional volume difference as

$$\left|\frac{\Delta V}{V}\right| = 2\left|\frac{h_{B2}-h_{B1}}{h_{B2}+h_{B1}}\right|, \tag{30}$$

where $h_{B1}=-34.4043$ eV Å^{-3} and $h_{B2}=-34.3978$ eV Å^{-3} are the specific enthalpies of the two phases at 451 GPa. Thus a discrepancy of $\Delta V/V\times 10^{-4}\approx 0.02\%$ in the volume of either phase would correspond to a 200-GPa

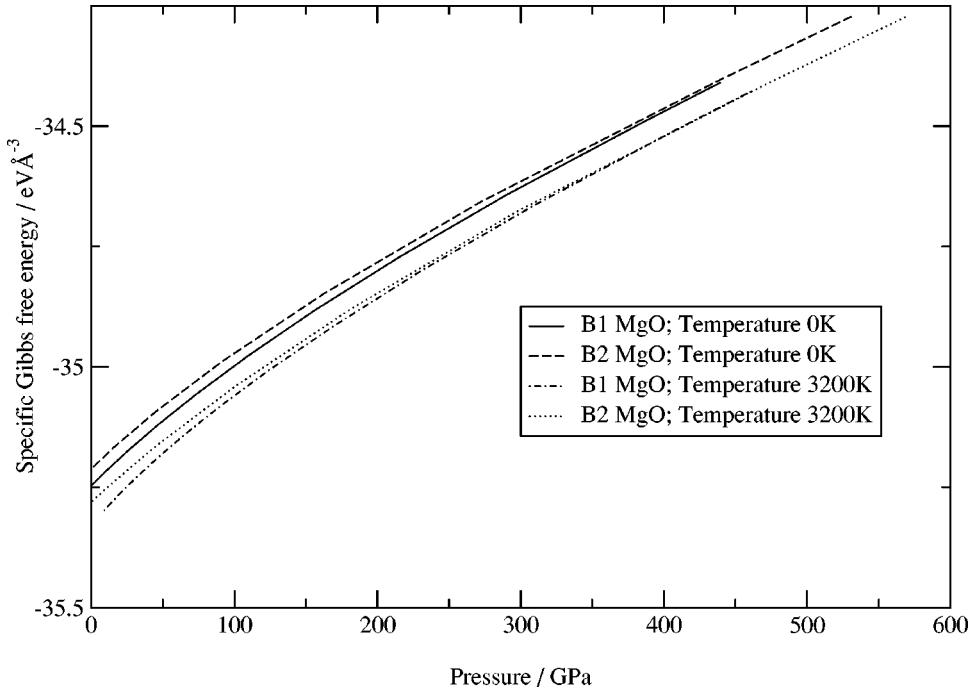

FIG. 10. Gibbs free energy plotted against pressure for the $B1$ and $B2$ phases of periclase at two different temperatures. The transition pressure at each temperature corresponds to the point where the curves cross. The similarity of the curves for each phase means that small errors in the energies lead to large uncertainties in the transition pressures.

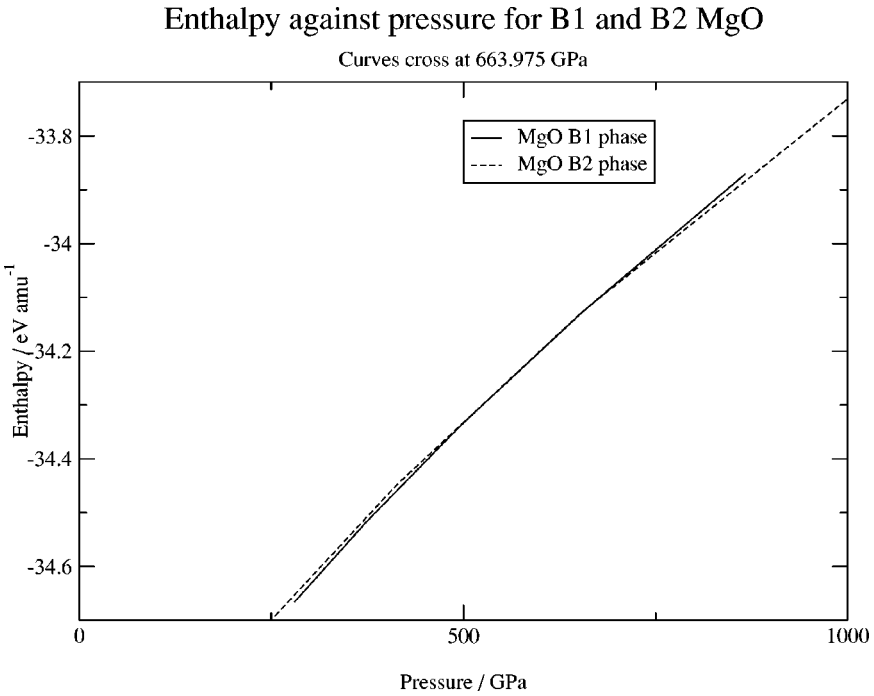

FIG. 11. Enthalpy $h=e+pv$ plotted against pressure for the $B1$ and $B2$ phases of MgO at a temperature 0 K (note that zero-point energy is not included in the results shown on this graph). The curves cross (and so the phase transition is predicted to occur) at 664 GPa. These results are obtained directly from the results of CASTEP. Note that, again, the two curves are extremely close when they cross; thus the position of the theoretical transition point is sensitive to the simulation parameters.

change in the transition pressure. This illustrates the sensitivity of the transition point to the details of how the total-energy calculations are carried out.

We use the generalized gradient approximation and ultrasoft pseudopotentials,[20,21] whereas Karki *et al.* used the local-density approximation and Q_c-tuned pseudopotentials.[32,33] The difference between calculated volume using these two methods is typically of the order of 5%; hence this is likely to be responsible for the difference between our results and Karki *et al.*'s.

The Clausius-Clapeyron equation for the coexistence line between two phases in (p,T) space is

$$\frac{dp}{dT}=\frac{\Delta s}{\Delta v}, \tag{31}$$

where $p(T)$ is the coexistence line and Δs and Δv are the specific entropy and volume differences between the two phases across the line. At zero temperature the entropy of the two phases should be zero by the third law of thermodynamics which is valid within our method (though not, e.g. in classical molecular dynamics[31]); therefore, provided the phases have different densities, the coexistence line should satisfy $dp/dT=0$ at $T=0$. Fig. 9) does not appear to satisfy this requirement.

The explanation for this apparent discrepancy lies with the fact that the densities of the two phases are very similar (and converging) at their predicted zero-temperature transition point: the specific volumes of the $B1$ and $B2$ phases are 0.202 and 0.198 $\text{Å}^3\text{amu}^{-1}$, respectively.

V. CONCLUSIONS

We have described an extension to the quasiharmonic method that allows the free-energy contribution from ''soft'' phonons in dynamically stabilized crystals to be evaluated. Our approach is based on a form of potential double-well different for that used in previous work on soft phonons: a parabola-plus-Gaussian form that has the advantage of being harmonic in both the low- and high-temperature limits.

We argue that the first-order nature of the phase transitions found using our extended quasiharmonic method arises because of the coupling of the relevant phonon to strain in the crystal. Without this coupling, the transition would be second order. We have suggested a criterion for judging when a second-order soft-mode phase transition has occurred, taking into account the quantum-mechanical nature of the problem.

At energies less than the height of the central barrier in our symmetric potential double well, the allowed energy levels consist of near-degenerate pairs. Hence we suggest there must exist extremely low-frequency photon absorption peaks for soft-mode materials in their low-temperature phase, corresponding to photon-induced transitions between such pairs.

We have evaluated the equation of state and the phase boundary for the $B1$-$B2$ transition in periclase using *ab initio* calculations in the quasiharmonic approximation. We predict that this transition will occur, but that it is well outside the ranges encountered inside the Earth. Locating the $B1$-$B2$ phase boundary with precision is difficult, however, because the Gibbs free energy curves of the two phases are very similar when they cross.

ACKNOWLEDGMENTS

We would like to thank D. C. Swift and M. C. Warren for helpful discussion. This work was carried out as part of the UKCP-MSI collaboration, supported by EPRSC GR/N02337. Copies of the codes used for the free-energy calculations are available from the authors on request.

[1] D. C. Wallace, *Thermodynamics of Crystals* (Wiley, New York, 1972).
[2] M. Born and K. Huang, *Dynamical Theory of Crystal Lattices* (Oxford University Press, London, 1956).
[3] W. Zhong, D. Vanderbilt, and K.M. Rabe, Phys. Rev. B **52**, 6301 (1995).
[4] M.C. Warren, G.J. Ackland, B.B. Karki, and S.J. Clark, Miner. Mag. **62**, 585 (1998).
[5] B.B. Karki, G.J. Ackland, and J. Crain, J. Phys.: Condens. Matter **9**, 8579 (1997).
[6] M.C. Warren and G.J. Ackland, Phys. Chem. Miner. **23**, (1996).
[7] M. C. Warren, Ph.D. thesis, The University of Edinburgh, 1997.
[8] G. Fiquet, A. Dewaele, D. Andrault, M. Kunz, and T. Le Bihan, Geophys. Res. Lett. **27**, 21 (2000).
[9] K. Parlinski and Y. Kawazoe, Eur. Phys. J. B **16**, 49 (2000).
[10] A.R. Oganov, J.P. Brodholt, and G.D. Price, Phys. Earth Planet. Inter. **122**, 277 (2000).
[11] G.J. Ackland, M.C. Warren, and S.J. Clark, J. Phys.: Condens. Matter **9**, 7861 (1997).
[12] K. Parlinski, J. Łażewski, and Y. Kawazoe, J. Phys. Chem. Solids **61**, 87 (2000).
[13] N. W. Ashcroft and N. D. Mermin, *Solid State Physics* (Saunders College Publishing, Philadelphia, 1976).
[14] W. Cochran and R.A. Cowley, J. Phys. Chem. Solids **23**, 447 (1962).
[15] D. C. Swift and G. J. Ackland, Phys. Rev. B **64**, 214107 (2001); D. C. Swift, Ph.D. thesis, The University of Edinburgh, 2000.
[16] A.D. Bruce, Adv. Phys. **29**, 117 (1980).
[17] L. Stixrude and R.E. Cohen, Nature (London) **364**, 613 (1993).
[18] P.E. Blöchl, O. Jepsen, and O.K. Andersen, Phys. Rev. B **49**, 16 223 (1994).
[19] CASTEP 3.9, academic version, licensed under the UKCP-MSI Agreement www.cse.clrc.ac.uk/Activity/UKCP (1999).
[20] J.P. Perdew, J.A. Chevary, S.H. Vosko, K.A. Jackson, M.R. Pederson, D.J. Singh, and C. Fiolhais, Phys. Rev. B **46**, 6671 (1992).
[21] D. Vanderbilt, Phys. Rev. B **41**, 7892 (1990).
[22] M.C. Payne, M.P. Teter, D.C. Allan, T.A. Arias, and J.D. Joannopoulos, Rev. Mod. Phys. **64**, 1045 (1992).
[23] H.J. Monkhorst and J.D. Pack, Phys. Rev. B **16**, 2981 (1977).
[24] K. Kunc, R. J. Needs, O. J. Nielsen, and R. M. Martin (unpublished).
[25] G. Peckham, Proc. Phys. Soc. London **90**, 654 (1967).
[26] Apart from the nonanalytic dipole term, which is calculated separately.
[27] M.J.L. Sangster, G. Peckham, and D.H. Saunderson, J. Phys. C **3**, 1026 (1970).
[28] H.J. Reichmann, S.D. Jacobsen, S.J. Mackwell, and C.A. McCammon, Geophys. Res. Lett. **27**, 799 (2000).
[29] I. Jackson and H. Niesler, in *High Pressure Research in Geophysics*, edited by S. Akimoto and M.H. Manghnani (Center for Academic Publication, Tokyo, 1982), pp. 93–113.
[30] T.S. Duffy, R.J. Hemley, and H.-K. Mao, Phys. Rev. Lett. **74**, 1371 (1995).
[31] A. Strachan, T. Çağin, and W.A. Goddard, Phys. Rev. B **60**, 15 084 (1999).
[32] J.P. Perdew and A. Zunger, Phys. Rev. B **23**, 5048 (1981).
[33] J.S. Lin, A. Qteish, M.C. Payne, and V. Heine, Phys. Rev. B **47**, 4174 (1993); M. H. Lee Ph.D. Thesis, University of Cambridge, UK, 1995.
[34] In fact, if we have calculated the total energy of the high-symmetry phase (corresponding to zero amplitude of the phonon) then we only need to carry out a further two frozen phonon calculations.